Probe Diagnostics in a Bismuth Hall Thruster

IEPC-05-129

Alex Kieckhafer[*], Dean Massey[†], and Lyon B. King[‡]
Michigan Technological University
815 R.L. Smith Bldg
Houghton, MI 49931

Abstract: **This paper reports on the status of on-going research to characterize the plume of a bismuth Hall thruster. Diagnostics for ion energy, multiply charged ion fractions, and beam divergence are developed for a 2-6 kW device. The apparatus includes a tungsten Faraday probe, a four-grid Retarding Potential Analyzer, and an ExB probe. The effects of bismuth plating, including change in secondary electron emission of current collectors and occlusion of RPA and ExB probe orifices and grids are examined. While data was unavailable at the time of writing, methods and error analyses are presented.**

Nomenclature

a	=	Acceleration parallel to the electric field (m/s^2)
$\vec{B}$	=	Magnetic field (T)
$\vec{E}$	=	Electric field (N/c)
$\vec{F}$	=	Net force on an ion (N)
J_i	=	Ion Current Density (mA/cm^2)
J_m	=	Measured Ion Current Density (mA/cm^2)
l	=	Distance between plates C2 and F (m)
l_c	=	Distance between plates C1 and C2 (m)
m	=	Ion mass (kg)
O_{C1}	=	Orifice diameter of plate C1 (m)
O_{C2}	=	Orifice diameter of plate C2 (m)
O_F	=	Orifice diameter of plate F (m)
q	=	Charge of an ion (c)
t	=	Time required for travel from plate C2 to plate F (s)
$\vec{v}$	=	Velocity (m/s)
v_l	=	Velocity parallel to the probe axis (m/s)
$\vec{v}_o$	=	Optimal velocity (m/s)
v_p	=	Velocity parallel to the electric field (m/s)
y	=	Displacement parallel to the electric field (m)
$\gamma(<E>)$	=	Secondary Electron Yield for ions of average energy $<E>$ (electrons/ion)
θ	=	Ion entry angle (radians)

[*] Graduate Research Assistant, Mechanical Engineering-Engineering Mechanics Department, awkieckh@mtu.edu
[†] Graduate Research Assistant, Mechanical Engineering-Engineering Mechanics Department, drmassey@mtu.edu
[‡] Assistant Professor, Mechanical Engineering-Engineering Mechanics Department, lbking@mtu.edu

1

I. Introduction

Bismuth shows significant promise as a propellant for high-power Hall thrusters.[1,2] The condensible nature that makes bismuth economically attractive for ground testing presents problems with spacecraft interactions, however. As bismuth may form an opaque, conductive coating on optics and dielectrics, determination of the plume characteristics of a bismuth Hall thruster is critically important. The same deposition properties that make plume characterization so important make the necessary probe diagnostics potentially more difficult. Any probe used to investigate a bismuth thruster plume must be able to tolerate deposition of bismuth on electrode and insulator surfaces.

The effect of a xenon Hall thruster plume on exposed spacecraft surfaces has been the subject of significant research. Experiments performed by Randolph,[3] Kusamoto,[4] and others utilized Faraday probes to measure the beam divergence of thrusters and thus the off-axis angle at which spacecraft surface erosion becomes significant. Measurements with a retarding potential analyzer (RPA) by Absalamov,[5] King,[6] and others determined the energy profile of the ions in the exhaust plume. ExB probe measurements taken by Kim[7] and more recently by Hargus[8] allowed further examination of the ion energy profile, as well as determination of the ratio of singly-charged to multiply-charged ions. Studies by Kim[9] and Domonkos[10] have also focused on very near-field behavior of thrusters. End-of-life behavior of thrusters has been studied by Pencil[11] and others. Exotic probes have also been employed, such as the parallel-plate electrostatic energy analyzer developed by Hofer and Haas,[12] based on the Molecular Beam Mass Spectrometer developed by King.[13] The purpose of these probe studies of the Hall thruster plume was to determine the nature of spacecraft interaction and develop an understanding of the ionization and acceleration processes in a Hall thruster.

A limitation to previous experimentation on xenon Hall thrusters, however, is that a bismuth Hall thruster may be significantly different from a xenon Hall thruster, thus mandating that plume studies be performed to determine the effect, if any, the conversion has on the plume and performance of the thruster. As the internal geometry of a bismuth thruster may also be different, there may be differences in the plume characteristics from typical SPT- or TAL-type thrusters. Studies of a thruster with internal geometry similar to a bismuth thruster during xenon operation have shown the beam profile is very similar to conventional xenon thrusters.[14] It is unknown how the ion energy or the fraction of multiply charged ions will be different from a xenon Hall thruster.

The fraction of ions in each charge state is expected to be different for a bismuth thruster. Bismuth has a lower secondary ionization energy than xenon, which indicates that if the discharge plasma conditions are otherwise identical bismuth should produce more multiply charged ions than xenon. As multiply charged ions are a source of inefficiency to a thruster, determination of the fraction of multiply charged ions is of significant importance to future thruster designs.

Bismuth plating may also present difficulties to probe operation. Any plating of bismuth on probe dielectrics will be disastrous to probe function, as it will nullify or reduce the insulating properties of these materials. Probe surfaces dependent on secondary electron yield may also be affected, as the secondary electron yield of bismuth is undoubtedly different than the tungsten, steel, or other materials typically used in probe construction. Occlusion of orifices may also be a problem on probes that utilize grids or apertures. Of these potential issues of bismuth deposition, only a change in secondary electron yield can be dealt with efficiently, as any change can be eliminated through a mathematical adjustment to the data. Coatings on dielectrics and/or apertures or grids may be disastrous, as either would severely limit the usefulness of the probe.

II. Goal of Research

The primary goal of the research presented here is to determine the characteristics of the plume of a bismuth Hall thruster. Of primary interest are the beam divergence, ion energy, and multiply charged ion fractions. The divergence of the thruster beam will be measured with a Faraday probe, while a Retarding Potential Analyzer (RPA) will measure the ion energy, and an ExB probe will measure the ion energy and multiply-charged ion fractions.

A secondary goal of this research will be to determine the effect bismuth has on the operation of Faraday, RPA and ExB probes. As bismuth is prone to plating of surfaces inside the test facility, it is expected that it will play a role in the function of the probes as conductive and dielectric surfaces become coated with bismuth. Occlusion of orifices in an ExB probe and the grids in an RPA will also be examined.

III. Theoretical Basis

A. Faraday Probe

A Faraday probe consists of a flat electrode, which is optionally surrounded by a guard electrode. The purpose of the guard electrode is to ensure the potential profile at the face of the probe is as flat as possible, preventing ions from being deflected to the side of the probe face by an off-axis electric field. The probe and guard electrode are typically biased several volts below the floating potential, such that the probe will only collect ions and repel electrons. Faraday probes are typically made of tungsten, as it has a very low secondary electron yield, reducing the potential error in measurements.

Calculation of the ion current density from a Faraday probe requires dividing the collected current by the face area of the probe, and modifying the resultant current density to reflect the secondary electron yield. The secondary electron yield is accounted for through the equation:[10]

$$J_i = J_m - \gamma(\langle E \rangle)J_m .$$
(1)

The value of γ is inherent to the probe material, and may change if the probe becomes coated with bismuth.

B. Retarding Potential Analyzer

An RPA is a gridded probe that uses electric fields to act as an energy filter.[15] Typical RPAs contain two to four grids, as in Figure 1. The first grid, at the entrance of the probe, either is allowed to float or is grounded. This serves to shield the plasma from the potentials inside the probe, and minimizes the disturbance to the plasma. The second grid is biased negative relative to the plasma potential. This serves as an electron repeller; ensuring only ions enter the probe. The third grid is an ion repeller. This grid has a variable, strongly positive potential applied to it. By adjusting the potential on this grid, ions of energies below the grid voltage are repelled and prevented from being detected. A fourth grid may be added after the ion repeller, which is biased negative to prevent secondary electrons from the current collector from escaping. The collector can be biased negative to serve as an ion attractor, but can also be grounded. Two-grid RPAs utilize only the electron repeller and ion repeller grids, and rely on knowledge of the secondary electron emission characteristics of the collector in place of the secondary electron suppression grid.
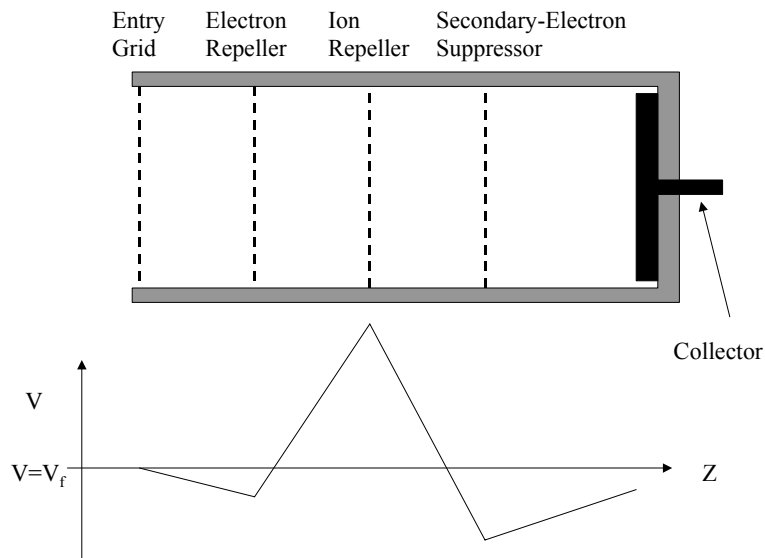

Figure 1: Diagram of RPA and potential structure within the probe. V_f is the floating potential of the plasma.

As an RPA is purely electrostatic in nature, it cannot differentiate between singly charged and multiply charged ions. The current measurements of an RPA are not dependent on ion energy, but rather the energy per unit charge on the ion. Thus a singly-charged ion with 300 eV of energy and a doubly-charged ion of 600 eV of energy will be filtered by the probe identically, preventing any differentiation of the charge state of ions. The benefit of an RPA is the probe does not require calibration. Ions are accepted or rejected based only on their energy and the potential applied to the ion repeller grid.

C. ExB Probe

An ExB probe utilizes perpendicular electric and magnetic fields to filter ions based on velocity. The magnetic field acts to divert ions away from an orifice, while the electric field provides an opposing force to push the ions back to their original path. The net force on an incident ion is given by:

$$\vec{F} = q\left[\left(\vec{v} \times \vec{B}\right) + \vec{E}\right]. \tag{2}$$

Where $\vec{F}$ if the force experienced by an ion, q is the charge of the ion, $\vec{v}$ is the velocity of the ion, $\vec{B}$ is the magnetic field in the probe, and $\vec{E}$ is the electric field in the probe. The velocity for which an ion will experience no net electromagnetic force is:

$$\vec{v}_o = \frac{\vec{E}}{\vec{B}}. \tag{3}$$

This relation allows ions of a specific velocity to pass through the probe on a straight-line trajectory, as the magnetic Lorenz force will be equal and opposite to the applied electric force. Ions of other velocities will not be able to pass, as they will either be diverted too much by the magnetic field, or not enough to counteract the electric force. A more complete explanation of the construction and theory of an ExB probe is presented elsewhere.[16]

In an ideal probe, only ions with velocity $\vec{v}_o$ will pass through the probe and be detected. This is not possible, however, as the entry and exit orifices of the filter are of a finite size, and an ion that enters the probe with a velocity at an angle to the probe axis may be deflected back into line with ions that enter parallel to the axis, as shown in Figure 2.
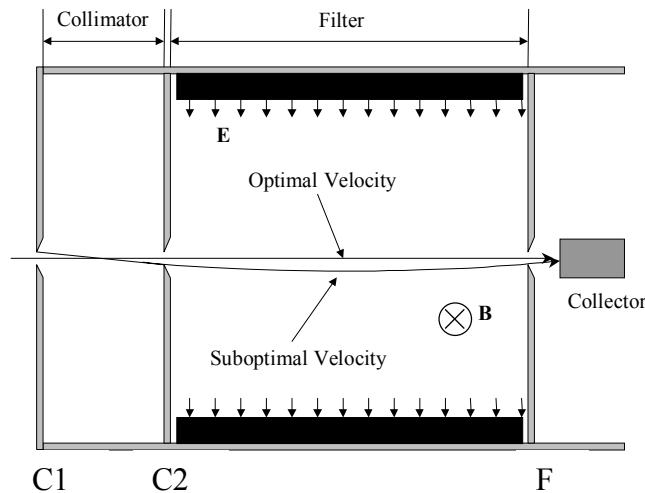
Figure 2: Schematic view of ExB probe. Plate C1 is the front plate of the probe, C2 is the filter entry or collimator exit plate, and F is the filter exit plate.

Both the velocity and position of a non-optimal ion must be considered to determine if it will be detected by the probe. The position is important because an ion that may be deflected just enough not to pass if it were on axis may

be deflected into the exit orifice of the filter and be detected. Velocity is important because an ion that is slightly faster or slower than the optimal velocity may not be deflected enough to prevent its detection. There are three components of velocity; parallel to the probe axis, parallel to $\vec{E}$, and parallel to $\vec{B}$. The velocity parallel to the probe axis is most important in determining if the ion will be detected; it is much larger than the other components and thus has much more of an effect on the magnetic force experienced than either of the other velocity components.

In order to determine the off-axis angle and position with which an ion can enter the filter section of the ExB probe, the orifice size and spacing in the collimator section must be taken into account, as ions of only a small entry angle and off-axis distance can enter the filter. The largest distance off-axis the ion can enter is one-half the diameter of the orifice in plate C2; larger off-axis distances will impact plate C2 and never enter the filter. The largest entry angle allowed is determined by an ion entering at one side of the orifice in plate C1 and traveling unobstructed to the other side of the orifice in plate C2. The angle is given by the equation:

$$\theta = \arctan\left(\frac{O_{C1} + O_{C2}}{2l_c}\right) \tag{4}$$

where O_{c1} is the diameter of the orifice in plate C1, O_{c2} is the diameter of the orifice in plate C2, and l_c is the distance between plates C1 and C2.

Ions with components of velocity parallel to $\vec{B}$ will be detected only if that velocity component is small enough that the ion would pass through the filter if no electric or magnetic field were present, since velocity parallel to $\vec{B}$ is unaffected by either the electric or magnetic field. Thus the filter acts as a very large collimator, allowing ions with extremely small off-axis angles to pass, as the allowable angle (given no obstruction from the orifice in plate C2) will be the found by $\theta = \arctan\left((O_{C1} + O_F)/2l_c\right)$, where OF is the diameter of the orifice in plate F.

Ions with components of velocity parallel to $\vec{E}$ are much harder to account for. Velocity along $\vec{E}$ can be changed by the fields in the filter, thus an ion with a total velocity different from $\vec{v}_o$ may be able to pass through the filter and be detected. In order to determine the range of ion velocities that allow such a trajectory, the acceleration of an ion under a nonzero sum of electromagnetic forces must be examined. For the purposes of this analysis, only the component of velocity parallel to the axis of the probe will be used to calculate magnetic force, as this component is nearly unaffected by either E or B, and is much larger than the other components of velocity given a small entry angle. As the component of velocity used to calculate the magnetic force is unaffected by that force, it can be assumed that the magnetic force is constant. Since the electric force does not change, the total acceleration can be assumed constant.   Due to the combination of the assumed-constant acceleration due to the magnetic field and the constant acceleration due to the electric field, equation (2) can be combined with the general equation for the motion of a particle under constant acceleration:

$$y = \frac{1}{2}at^2 + v_p t \tag{5}$$

to give:

$$y = \frac{qt^2}{2m}\left(v_l B + E\right) + v_p t \;. \tag{6}$$

where y is the off-axis distance, m is the mass of the ion, v_l is the component of velocity parallel to the axis of the probe, v_p is the component of velocity parallel to the electric field, and t is time. The components of velocity are calculated using the maximum possible entry angle, as calculated in equation (4). As the displacement of the ion at the end of the filter is of greatest importance, t becomes the time required for the ion to traverse the filter section, which is expressed as the length of the filter divided by the velocity parallel to the probe axis. Thus, a substitution can be made into equation (6) to produce:

$$y = \frac{ql^2 B}{2mv_l} + \frac{ql^2 E}{2mv_l^2} + \frac{v_p l}{v_l} \;. \tag{7}$$

The equation can be further simplified by replacing the velocity components with expressions based on the total velocity:

$$y = \frac{ql^2 B}{2mv\cos(\theta)} + \frac{ql^2 E}{2mv^2\cos^2(\theta)} + \frac{vl\sin(\theta)}{v\cos(\theta)} \ . \tag{8}$$

This change in variables removes the velocity dependence from the third term of the equation, which can now be trivially rearranged to:

$$2m\cos^2(\theta)(y - l\tan(\theta))v^2 - ql^2 B\cos(\theta)v - ql^2 E = 0 \ . \tag{9}$$

The value of y to use in this equation is the total distance an ion can travel parallel to the electric field, assuming it enters at one side of the orifice in plate C2 and exits at the other side of the orifice in plate F. By substituting the average of the orifice sizes in plates C2 and F for y, equation (9) becomes a quadratic equation for v. Since θ can be positive or negative, maximum and minimum possible velocities can be calculated by changing the polarity of θ. The maximum and minimum velocities are not necessarily the same distance from the optimal velocity, and must be calculated separately.

Measurement of ion energy by an ExB probe requires calibration. Magnetic and electric fields are difficult to measure with enough precision to make energy measurements, thus calibration by other means is necessary. Typically the measurements of an ExB probe are correlated with those from an RPA or other electrostatic energy analyzer. A single-point calibration may be obtained by matching the peak of the distribution generated by an RPA with the energy of the singly charged ion peak in an ExB probe. As the filtering effect is linear with increasing velocity, a zero applied electric field will allow ions of zero energy to pass; thus the two point requirement for a linear fit is met, and ion energy measurements can be taken with the probe.

IV. Experimental Apparatus

A. Thruster

To allow for the controlled flow of bismuth propellant to the discharge of a Hall thruster, a method has been developed which utilizes the waste heat of the thruster to maintain the anode at sufficient temperatures for bismuth evaporation.[17] Thermal control of anode temperature is accomplished through the use of inert shim electrodes, which allow thermal control through control of discharge current attachment. Shifting current from anode to shims will cool the anode due to the reliance on the discharge current for heating. The discharge current is shifted by reducing the shim voltage below the voltage on the main anode. Control of the anode temperature will control the evaporation rate of bismuth through a change in vapor pressure, which will thus control the propellant mass flow into the thruster.

The bismuth thruster to be used for the experiments reported here consists of the magnetic circuit of an Aerojet BPT-2000 thruster[18], with the single anode replaced with a dual-mode anode and shim electrodes.[17] The dual-mode anode is divided into two chambers: the lower chamber is connected to a xenon flow control system and allows operation and warm-up on xenon while bismuth vapors are allowed to escape through a diffuser plate on the front face of the anode. This allows the thruster to be started without external heat, and thus ensures the thruster can maintain the absolute temperatures required for bismuth operation. A cross-section of such a thruster is shown in Figure 3.
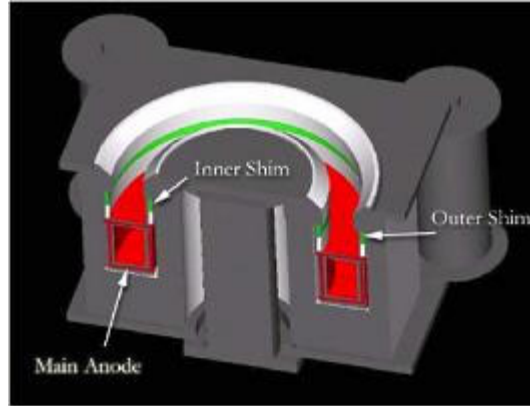
**Figure 3: Cross Section of segmented-electrode Hall thruster**

B. Facility

Experiments with xenon as propellant were performed[19] in Isp Lab's xenon Test Facility (XTF), shown in Figure 4. The facility is comprised of a 2-m-diameter by 4-m-long vacuum tank. Rough pumping is accomplished by a two-stage rotary oil-sealed vacuum pump with a Roots blower, capable of pumping at 400 cfm. High vacuum is achieved through dual 48-inch-diameter cryopumps, capable of pumping 120,000 liters per second on nitrogen.
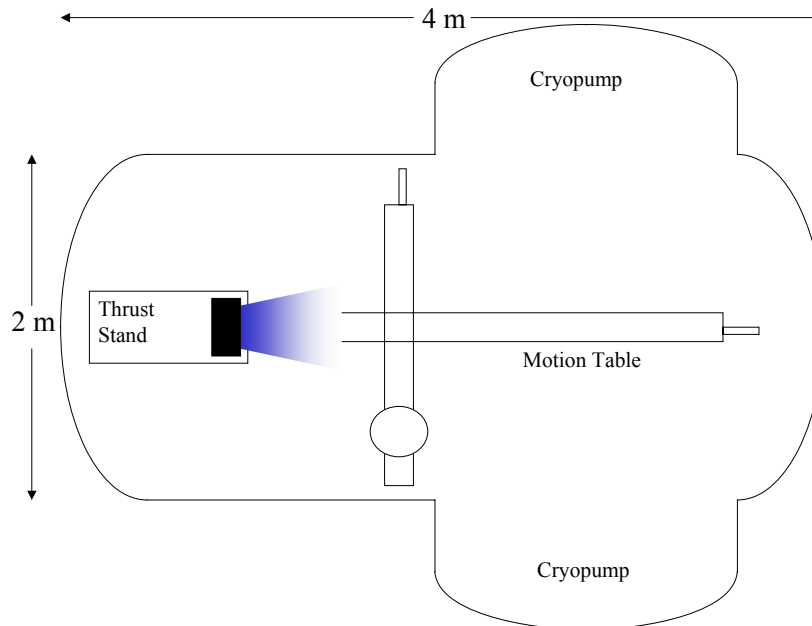
Figure 4: xenon Testing Facility

Bismuth experiments are performed in the bismuth testing facility (BTF), as shown in Figure 5. The facility consists of a 2-m-diameter, 4-m-long cylindrical vacuum tank. Rough pumping is accomplished through a two-stage mechanical pump, capable of 400 cfm. High vacuum is achieved through the use of three Leybold MAG-2000 turbomolecular pumps, with a combined throughput of 6,000 l/s, and providing a base pressure below 10^{-6} Torr.
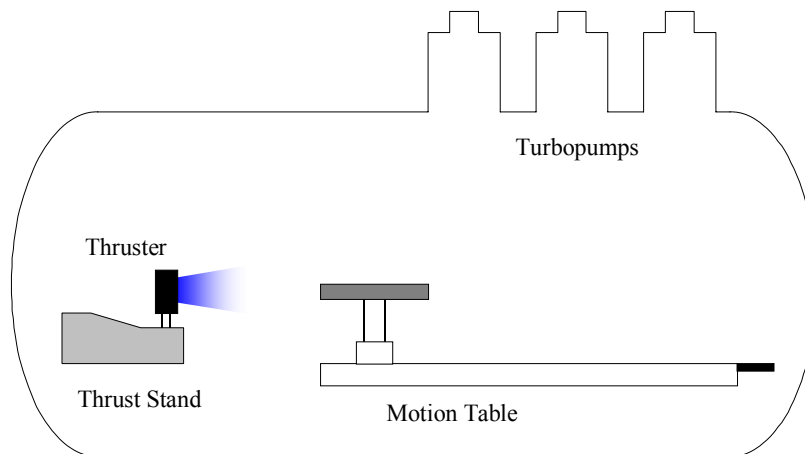
Figure 5: Diagram of the Bismuth Testing Facility

C. Faraday Probe

The Faraday probe consists of a 2.4-mm-diameter tungsten collector, enclosed in an alumina sheath with an outer diameter of 4.75 mm. A steel guard ring with a diameter of 10 mm is included to reduce edge effects on the potential structure in front of the probe face. Both the probe and guard ring are biased to the same potential, in the ion saturation regime below the floating potential. The probe is swept across the face of the thruster at a constant radius, using the exit plane of the thruster as zero point. Motion of the probe will be accomplished by use of a motion table capable two-dimensional horizontal motion as well as rotation about the vertical axis. Sweeps are performed at radii of 250 and 500 mm. Secondary electron yields will be estimated from experimental data.[20] Average ion energies used in determination of the secondary electron yield will be based on the RPA measurements.

D. RPA

The RPA utilizes a four-grid design, with a 12.7-mm-diameter collector area. The grids are made of stainless steel, and have open area fractions of roughly 34%, with hole sizes on the order of 0.1 mm. The entry or shield grid will be either grounded or held at the plasma potential as measured by a Langmuir probe. The current collector will consist of a stainless steel disc.

E. ExB Probe

The ExB probe has a 5 cm collimator (distance between plates C1 and C2), and 23 cm filter (distance between plates C2 and F). The orifices in plates C1 and C2 are 1.6 mm in diameter. The orifice in plate F is 0.8 mm in diameter. All of the orifices have 90-degree chamfers on their downstream sides, to prevent ions from hitting the interiors of the orifices and unnecessarily reducing the measured current. The magnetic field is supplied by six 5 cm x 7.6 cm x 1.3 cm grade 8 ceramic magnets, arrayed at the top and bottom of the probe, which provide an approximately 0.15 T field in the filter as measured by a magnetic field probe at the centerline of the filter. The magnets are separated by Teflon spacers, which also hold and insulate the electrode plates from the structure of the probe. The current is read by a K and M Electronics model 7550m channel electron multiplier. The multiplier will be operated at supply voltages up to –2350 V, which correlates to a gain of up to 10^8. The casing of the probe as well as the three orifice plates are fabricated of magnetic stainless steel, to direct and focus the magnetic field while preventing oxidation as is typical of magnetic iron or mild steels. The magnetic field outside the filter section of the probe is less than one gauss. The output current of the electron multiplier will be converted to a voltage signal via a 1M Ohm resistor and displayed on an oscilloscope. Tuning of the electrodes and thus the electric field in the probe

8

will be performed by two power supplies controlled by a function generator. The electrodes will be swept through a roughly 120-volt difference at a rate of 2 Hz, which with the estimated magnetic field corresponds to an ion with nearly 2,700 eV of energy, well above the 2,400 eV expected of a quadruply-charged ion accelerated through a 600 V potential.

Application of the error analysis from section (III) yields an estimate of the uncertainty in ion velocity and energy measurements. Errors in energy measurements are plotted in Figure 6.
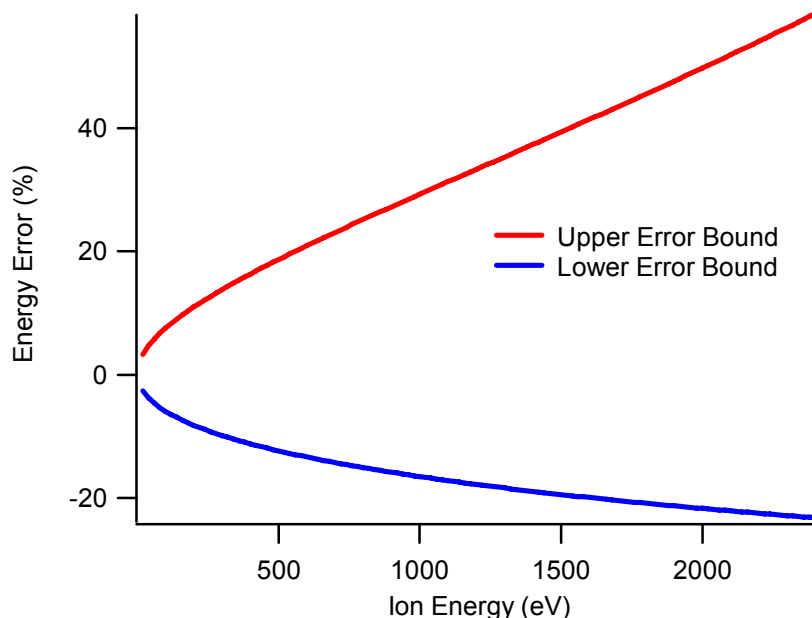
Figure 6: Error in Energy Measurements from the ExB probe

For an incident ion with 300 eV of energy, the error is estimated to be 13.8% (41.3 eV) at the upper bound and –9.9% (–29.6 eV) at the lower bound. These errors are quite large, and will make measurement of ion energy difficult. Reducing the error could be accomplished by addition of a drift tube and fourth orifice plate behind plate F, which would require ions not only be in a position to pass through plate F, but also have velocity such that they would pass through both plate F and the fourth plate. Accuracy could also be increased by reducing the diameter of one or more orifices.

V.   Results

Experimental results were not available at the time of the paper deadline. Results will be orally presented at the 2005 IEPC.

[1] Kieckhafer, A.W., and King, L.B., "Energetics of Propellant Options for High-Power Hall Thrusters," 41st Joint Propulsion Conference and Exhibit, 10-13 July 2005, Tucson, AZ, AIAA-2005-4228

[2] Massey, D.M., et. al, "Development of a Vaporizing Liquid Bismuth Anode for Hall Thrusters," 40th Joint Propulsion Conference, 11-14 July, 2004, Fort Lauderdale, FL, AIAA-04-3648

[3] Randolph, T., Pencil, E., and Manzella, D., "Far-Field Plume Contamination and Sputtering of the Stationary Plasma Thruster," 30th Joint Propulsion Conference, 27-29 June 1994, Indianapolis, IN, AIAA-94-2855

[4] Kusamoto, D., et. al., "Exhaust Beam Profiles of Hall Thrusters," ISTS-96-a3-09

[5] Absalamov, S.K., et. al., "Measurement of Plasma Parameters in the Stationary Plasma Thruster (SPT-100) Plume and its Effect on Spacecraft Components," 28th Joint Propulsion Conference, 6-8 July 1992, Nashville, TN, AIAA-92-3156

[6] King, L. B., and Gallimore, A. D., "A Gridded Retarding Pressure Sensor for Ion and Neutral Particle Analysis in Flowing Plasmas," Review of Scientific Instruments, **68**(2), Feb. 1997, p.1183-1188.

[7] Kim, S-W., and Gallimore, A.D., "Plume Study of a 1.35 kW SPT-100 Using an ExB Probe," 35th Joint Propulsion Conference, 20-24 June 1999, Los Angeles, CA, AIAA-99-2423

[8] J. Ekholm and W. Hargus, "ExB Measurements of a 200 W xenon Hall Thruster," 41st AIAA/ASME/SAE/ASEE Joint Propulsion Conference and Exhibit, Tucson, Arizona, July 10-13, 2005 AIAA 2005-4405

[9] Kim, S-W., et. al., "Very Near-Field Plume Study of a 1.35 kW SPT-100," 32nd Joint Propulsion Conference, 1-3 July, 1996, Lake Buena Vista, FL, AIAA-96-2972

[10] Domonkos, M.T., Marrese, C.M., et. al., "Very Near-Field Plume Investigation of the D55," 33rd Joint Propulsion Conference and Exhibit, July 6-9, 1997, Seattle, WA, AIAA-97-3062

[11] Pencil, E.J., et. al., "End-of-Life Stationary Plasma Thruster Far-field Plume Characterization," 32nd Joint Propulsion Conference, 1-3 July, 1996, Lake Buena Vista, FL, AIAA-96-2709

[12] Hofer, R.R, Haas, J.M., et. al., "Development of a 45-Degree Parallel-Plate Electrostatic Energy Analyzer for Hall Thruster Plume Studies: Preliminary Data," 26th International Electric Propulsion Conference, 17-21 October, 1999, Kitakyushu, Japan, IEPC-99-113

[13] King, L.B., Transport-property and Mass Spectral Measurements in the Plasma Exhaust Plume of a Hall-effect Space Propulsion System, Ph.D. Dissertation, University of Michigan, 1998.

[14] Kieckhafer, A.W., et. al., "Effect of Segmented Anodes on the Beam Profile of a Hall Thruster," 40th Joint Propulsion Conference, 11-14 July, 2004, Fort Lauderdale, FL, AIAA-04-4101

[15] Hutchinson, I.H., Principles of Plasma Diagnostics, Cambridge University Press, 1987, ISBN 0-521-38583-0

[16] Kim, S-W., Experimental Investigations of Plasma Parameters and Species-Dependent Ion Energy Distribution in the Plasma Exhaust Plume of a Hall Thruster, Ph.D. Dissertation, University of Michigan, 1999.

[17] Massey, D.M., et. al., "Progress on the Development of a Direct Evaporation Bismuth Hall Thruster," 41st Joint Propulsion Conference and Exhibit, 10-13 July 2005, Tucson, AZ, AIAA-2005-4232

[18] King, D., et. al., "Development of the BPT Family of U.S.- Designed Hall Current Thrusters for Commercial LEO and GEO Applications," 34th Joint Propulsion Conference, July 12-15, 1998, Cleveland, OH, AIAA-98-3338

[19] Kieckhafer, A.W., et. al., "Performance and Active Thermal Control of a 2-kW Hall Thruster with Segmented Electrodes", Journal of Propulsion and Power, submitted 10/2005

[20] Coomes, Edward A., "Total Secondary Electron Emission from Tungsten and Thorium-Coated Tungsten", Phys Rev (APS) **55**, March 1939